Nonlinear Spontaneous Oscillations at the Liquid/Liquid Interface Produced by Surfactant Dissolution in the Bulk Phase

N. M. Kovalchuk[†] and D. Vollhardt*[,‡]

Institute of Biocolloid Chemistry, 03142 Kiev, Ukraine, and Max Planck Institute of Colloids and Interfaces, D-14424 Potsdam/Golm, Germany

Received: August 9, 2005; In Final Form: October 11, 2005

The results of theoretical and experimental studies of spontaneous nonlinear oscillations produced at the liquid/liquid interface by surfactant transfer from a point source situated in one of the bulk phases are presented. The theoretical analysis is based on the direct numerical simulation of the system evolution. The experiments are performed for the heptane/water interface using middle-chain aliphatic alcohols as surfactants. The results for the oil/water interface are compared with the corresponding data obtained for the air/water interface. The presented results allow the conclusion that auto-oscillations at the air/liquid and liquid/liquid interfaces are governed by very similar mechanisms but their characteristics are strongly dependent on the properties of the two contacting media, in particular, on the surfactant partition coefficient.

Introduction

Spontaneous nonlinear oscillations arising at liquid interfaces by the solute transfer were intensively studied during the last three decades.[1−4] Some of the typical experimental systems wherein this phenomenon is observed are reviewed in ref 5. Pseudoperiodic oscillations of the interfacial tension and the electrical potential difference across the oil/water interface were observed when the water and oil phases, each containing an ionic solute (one of them is a surfactant), were brought in contact and the solutes began to transfer in the opposite directions through the interface (system 1).[1,2,6−12] Much more regular and well-shaped oscillation develops when solute transfer occurs between two water layers through an interposed oil layer (system 2). The liquid phases are placed in a U-shape tube[3,13−15] or in a system composed of a cylindrical vessel and a hollow tube inserted in the center of the vessel.[16,17] Another possibility to produce nonlinear spontaneous oscillation at the liquid interface is the use of only one transferred solute from the surfactant source in the bulk. Auto-oscillation of the surface tension was observed by dissolution of a surfactant droplet under the water surface (system 3),[18−21] and oscillation of the interfacial tension and of the electrical potential through the water/nitrobenzene interface occurs by gradual injection of an ionic surfactant in the bulk water (system 4).[22−25] The peculiarity of oscillations in all considered systems is their essential nonlinearity. Appearance of these oscillations cannot be explained in the frames of existing theories on the basis of the linear stability analysis.[26−29]

It is established that chemical interactions between transferred solutes are crucial for oscillations in systems 1 and 2. However, the correlations between the physicochemical and hydrodynamic processes and, therefore, the actual mechanisms underlying the behavior of these systems are not quite clear to date. System 3 is the simplest among the four considered systems, and the oscillation mechanism as well as the effect of the various system characteristics have been established for system 3 employing direct numerical simulation of the system evolution.[30−32] According to the developed theory, auto-oscillation of the surface tension is the result of Marangoni instability periodically arising and fading. The instability fades due to the interaction of the longitudinal wave, generated by instability, with the vessel wall.

The objective of the present work is to study to what extent the theory developed for air/liquid interface[30−32] is applicable also for the case of oscillations at the oil/water interface caused by the surfactant transfer from a point source situated in the bulk of the liquid. The results of experimental study of interfacial tension oscillation, produced at the heptane/water interface by dissolution of a medium-chain alcohol droplet in the water phase, are compared with the results of numerical simulations as well as with the experimental data obtained for the system with the medium-chain alcohol droplet under the air/water interface.

Mathematical Formulation. The geometry of the considered problem is shown in Figure 1. The model system represents a cylinder with the radius R_0 bound from below and above by rigid plates and containing two superimposed layers of immiscible viscous incompressible Newtonian liquids with different physical properties. The height of the lower liquid layer is H_{01}, and the height of the upper liquid layer is H_{02}. A cylindrical capillary with a spherical surfactant droplet on the tip is immersed in the liquids so that the capillary axis coincides with the vessel axis and the capillary edge is situated in the lower liquid at distance h from the interface. All variables are assumed to be independent of the angular coordinate according to the system symmetry and the experiments with flow visualization at the air/water interface. The temperature is assumed to be constant. All thermal effects are neglected. The system evolution is described by the Navier−Stokes continuity and convective diffusion equations rewritten in terms of vorticity and stream function in cylindrical coordinates. The dependence of the solution density on the surfactant concentration is taken into account only in the buoyancy term (Boussinesq approximation). By scaling time, length, velocity, concentration, stream

* To whom correspondence should be addressed. E-mail: vollh@mpikg-golm.mpg.de.
[†] Institute of Biocolloid Chemistry.
[‡] Max Planck Institute of Colloids and Interfaces.

10.1021/jp054452f CCC: $30.25
Published on Web 11/11/2005

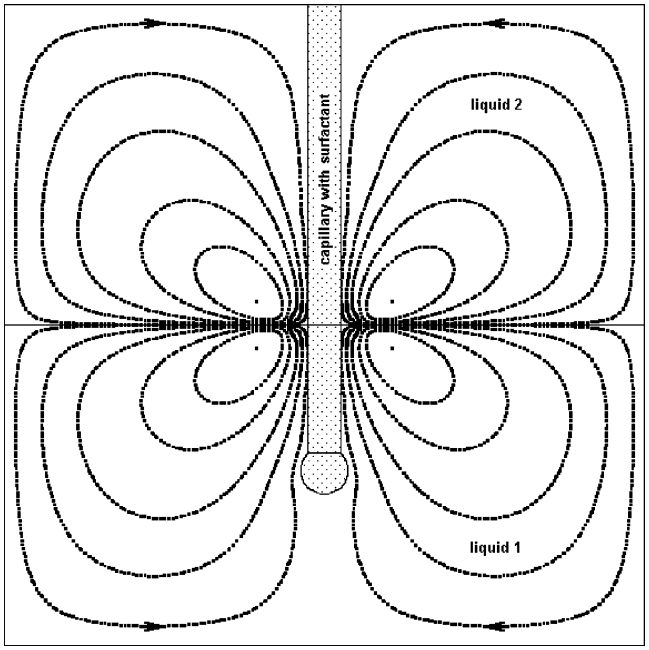

Figure 1. Scheme of the measuring cell with streamlines of quasi-steady Marangoni convection.

function, and vorticity correspondingly with L^2/D_1, L, D_1/L, c_{01}, LD_1, and D_1/L^2, the dimensionless form of the governing equations for each of the phases ($i = 1$ corresponds to the lower liquid, $i = 2$ to the upper liquid) is[33]

$$\frac{\partial \omega_i}{\partial t} + \frac{\partial (v_{ri}\omega_i)}{\partial r} + \frac{\partial (v_{zi}\omega_i)}{\partial z} - Sc_i \frac{D_i}{D_1}\left(\frac{\partial^2 \omega_i}{\partial r^2} + \frac{\partial^2 \omega_i}{\partial z^2} + \frac{1}{r}\frac{\partial \omega_i}{\partial r} - \frac{\omega_i}{r^2}\right) + Ra_i Sc_i \frac{D_i^2}{D_1^2}\frac{c_{01}}{c_{0i}}\frac{\partial c_i}{\partial r} = 0 \quad (1)$$

$$\frac{\partial^2 \Psi_i}{\partial r^2} + \frac{\partial^2 \Psi_i}{\partial z^2} - \frac{1}{r}\frac{\partial \Psi_i}{\partial r} - \omega_i r = 0 \quad (2)$$

$$\frac{\partial c_i}{\partial t} + \frac{\partial (v_{ri}c_i)}{\partial r} + \frac{\partial (v_{zi}c_i)}{\partial z} + \frac{v_{ri}c_i}{r} - \left(\frac{\partial^2 c_i}{\partial r^2} + \frac{\partial^2 c_i}{\partial z^2} + \frac{1}{r}\frac{\partial c_i}{\partial r}\right) = 0 \quad (3)$$

where L is a characteristic length scale, D_i is the bulk diffusion coefficient of the surfactant in the ith phase, c_{0i} is the surfactant solubility in the ith phase, the ratio $k_p = c_{02}/c_{01}$ is the partition coefficient of the surfactant, t is time, r is the radial coordinate, z is the normal to the interface coordinate downward directed with $z = 0$ on the interface, v_{ri} and v_{zi} are the velocity components in the radial and normal to the interface directions, respectively, Ψ_i is the stream function, defined so that $v_{ri} = 1/r\ \partial\Psi_i/\partial z$, $v_{zi} = -1/r\ \partial\Psi_i/\partial r$, $\omega_i = \partial v_{ri}/\partial z - \partial v_{zi}/\partial r$ is the vorticity, $Sc_i = \nu_i/D_i$ is the Schmidt number, $Ra_i = gc_{0i}L^3/\rho_{0i}\nu_i D_i\ \partial\rho_i/\partial c_i$ is the Rayleigh number, ν_i is the kinematic viscosity of the ith phase, $\rho_i = \rho_{0i} - (c_i/c_{0i})(\rho_{0i} - \rho_{si})$ is the solution density, ρ_{0i} is the density of the pure ith phase, ρ_{si} is the density of the saturated surfactant solution in the ith phase, g is the acceleration due to gravity, and c_i is the surfactant concentration.

In the initial state, the liquids are supposedly motionless. The dimensionless surfactant concentration is equal to unity at the droplet/solvent interface and is equal to zero elsewhere else. No-slip boundary conditions are used for the vessel wall, the capillary, and the droplet surface. The liquid interface is supposed to be nondeformable. The intrinsic surface viscosity is neglected. Diffusion-controlled adsorption kinetics is assumed. Local equilibrium is assumed between the surface concentration and the sublayer concentration. It is described by the Langmuir isotherm in dimensionless form

$$\Gamma = \frac{c_1}{1 + K_L c_{01} c_1} \quad (4)$$

The surfactant mass balance on the interface is described by the equation

$$\frac{\partial \Gamma}{\partial t} + \frac{\partial (\Gamma v_r)}{\partial r} + \frac{\Gamma v_r}{r} - \frac{D_S}{D_1}\left(\frac{\partial^2 \Gamma}{\partial r^2} + \frac{1}{r}\frac{\partial \Gamma}{\partial r}\right) - N_E\left(\frac{\partial c_1}{\partial z} - \frac{D_2}{D_1}\frac{\partial c_2}{\partial z}\right) = 0 \quad \text{at } z = 0 \quad (5)$$

Here, $N_E = L/K_L\Gamma_m$ is the exchange number that determines the effect of surfactant exchange between the surface and the bulk ($N_E \to 0$ corresponds to the limiting case of the insoluble monolayer when exchange with the bulk is absent), K_L and Γ_m are the parameters of the Langmuir isotherm related to liquid 1, D_S is the surface diffusion coefficient, and Γ is the Gibbs adsorption scaled by $c_{01}K_L\Gamma_m$.

Local equilibrium of the surfactant distribution between the liquid phases at the interface is also assumed

$$\frac{c_2}{c_1} = k_p \quad \text{at } z = 0 \quad (6)$$

The boundary condition for the vortex on the free surface is obtained from the tangential stress balance employing the Szyszkowsky−Langmuir equation for the state of the adsorbed surfactant

$$\omega_1 = \frac{\rho_{02}\nu_2}{\rho_{01}\nu_1}\omega_2 + Ma\frac{1}{(1 - K_L c_0 \Gamma)}\frac{\partial \Gamma}{\partial r} \quad \text{at } z = 0 \quad (7)$$

Here, $Ma = RTc_{01}K_L\Gamma_m L/\rho_{01}\nu_1 D_1$ is the Marangoni number, R is the gas constant, and T is the temperature.

As a second boundary condition for the vortex, we used the continuity of the tangential velocity component at the interface

$$v_{r1} = v_{r2} \quad \text{at } z = 0 \quad (8)$$

For convenience, the results are presented in dimensional form. The following values are used for the geometrical parameters: characteristic length $L = R_0 = H_{01} = H_{02} = 20$ mm, capillary radius $r_c = 1$ mm, and droplet radius $r_0 = 1.5$ mm. The surfactant properties are chosen corresponding to the properties of the system with an octanol droplet under the air/water interface:[19] $c_0 = 3.4$ mol/m^3 for the solubility of the surfactant, $K_L = 3.23$ m^3/mol, $\Gamma_m = 6.6 \times 10^{-6}$ mol/m^2 for the parameters of the Langmuir isotherm, $D_1 = 6.7 \times 10^{-6}$ cm^2/s for the volume diffusion coefficient, and $D_s = 6.7 \times 10^{-6}$ cm^2/s for the surface diffusion coefficient. The lower phase is water (density $\rho_1 = 1$ g/cm^3, solution kinematic viscosity $\nu_1 = 0.01$ cm^2/s). The density difference $\Delta\rho_s$ between water and saturated surfactant solution is chosen with $\Delta\rho_{s1} = 10^{-5}$ g/cm^3. If not otherwise stated, the properties of the upper phase are chosen as follows: $D_2 = 6.7 \times 10^{-6}$ cm^2/s, $\rho_2 = 0.99999$ g/cm^3, $\nu_2 = 0.01$ cm^2/s, $\Delta\rho_{s2} = 0$, and capillary immersion depth, $h = 10$ mm.

TABLE 1: Dependence of the Auto-oscillation Characteristics on the Grid Resolution

grid resolution	induction period, min	oscillation period, min[a]	oscillation amplitude, mN/m[a]
80 × 80	17.5	10.25	1.71
100 × 100	18.4	9.91	1.80
120 × 120	19.1	9.61	1.81

[a] The mean value for the third−sixth oscillations.

The governing equations with the corresponding boundary conditions are used for the numerical simulation of the system evolution. Equation 2 was solved by the Gauss−Seidel iterative method. In eqs 1 and 3, the two-point forward difference approximation is used for the time derivatives, the three-point centered differences are used for the diffusion terms, and the modified upwind differences are used for the convective terms.[34]

Our previous numerical studies concerning the droplet dissolution under the air/water interface were performed employing the grid resolution 80 × 80 in the absence of buoyancy and 120 × 120 by accounting for the buoyancy effect.[30,33] To implement the proper grid resolution for this study, we calculated the main oscillations characteristics for three different grids (Table 1) using the parameter value given above, except the droplet radius, which was taken as $r_0 = 2$ mm for a correct presentation of the droplet in all grids. The capillary immersion depth, h, was $h = 14$ mm, the properties of the upper phase coincide with those of the lower phase, and the surfactant distribution coefficient, k_p, was $k_p = 1$. For the convenience of the comparison with previous results obtained for the air/liquid interface, the surfactant properties are chosen corresponding to the properties of the system with an octanol droplet under the air/water interface:[19] $c_0 = 3.4$ mol/m^3 for the surfactant solubility, $K_L = 3.23$ m^3/mol, $\Gamma_m = 6.6 \times 10^{-6}$ mol/m^2 for the parameters of the Langmuir isotherm, $D_1 = 6.7 \times 10^{-6}$ cm^2/s for the volume diffusion coefficient, and $D_s = 6.7 \times 10^{-6}$ cm^2/s for the surface diffusion coefficient. It is worth noting that the activity of octanol at the air/water interface is indeed rather close to its activity at the alkane/water interface (cf. Table 8).

It is seen from Table 1 that all the presented characteristics converge and the difference between the characteristics for grids 100 × 100 and 120 × 120 is less than 4%. Thus, in the present work, we used the grid 120 × 120 mesh points keeping in mind that we slightly underestimated the values of induction period and oscillation amplitude and slightly overestimated the values of oscillation period.

Experimental Section

The experimental studies of the surface tension oscillations at the oil/water interface were performed with the tensiometric setup described elsewhere[21] in a thermostated room at 22 °C. Ultrapure deionized water produced by "Purelab Plus" (20 mL) was placed at the bottom of a cylindrical glass vessel with an inner diameter of 40 mm. A cylindrical glass capillary with diameter of ∼2 mm was introduced to the desired depth in the water phase. A platinum Wilhelmy plate freshly annealed was fully submerged in the water. Then, 10 mL of heptane (Fluka, purity >99.5%, density 0.684 g/cm^3, dynamic viscosity 0.39 mPa·s) was gently poured onto the water surface. The Wilhelmy plate was lifted to the heptane/water interface, and the system was equilibrated during ∼3 h. Afterward, the surfactant droplet (hexanol or octanol) was formed at the tip of the capillary and the measurement of the interfacial tension was restarted.

Before it was used, the heptane surface was cleaned several times to remove surface-active contaminations. Measurements performed during 10 h at once after the interface formation showed that, during the first hour, the interfacial tension decreases ∼0.1 mN/m and then it remains constant. Therefore, there can be minor surface-active contaminations in the considered system, but their content is quite small.

Hexanol and octanol with a purity of >99.5% (Fluka) were used, as purchased.

The experiments at the air/water interface were performed in a glass vessel with diameter of 40 mm, as described in refs 19 and 21.

Results and Discussion

The presence of the second liquid phase instead of air should essentially affect the system evolution. First of all, the surfactant transfer through the liquid/liquid interface can be rather strong whereas the transfer into the air phase is usually negligible. For example, the distribution coefficient of *n*-heptanol between air and water at 22 °C is 1.13×10^{-4},[35] but that between octane and water at 20 °C is 8.55.[36] Surfactant transfer into the second liquid phase influences the formation of the concentration gradients in the system and therefore the development of instability. The dynamic viscosity of air is some orders of magnitude smaller than the dynamic viscosity of water or oil. Physically it means that, in the air/water system, chemical energy released due to the surface concentration gradient is spent to produce convection only in water phase, whereas in the oil/water system, the convection extends to both liquid phases. Therefore, the same interfacial concentration gradient leads to a smaller change of the momentum in the water phase of the oil/water system in comparison to the air/water system. An extension of the convection into the oil phase influences immediately the interfacial concentration gradients as well. For example, during the rise of instability, diluted surfactant solution is supplied from the oil bulk to the interface in the vicinity of the capillary. The performed numerical simulation displays clearly that all considered effects influence essentially the oscillation characteristics. Nevertheless, the dissolution of the surfactant droplet under the liquid/liquid interface (as well as the surfactant supply from another source with dimensions small enough in comparison to the dimensions of the interface, e.g., studied in refs 22−25) can result in oscillation of the interfacial tension produced by the mechanism similar to that proposed recently for auto-oscillation at the air/water interface.[30−32]

It was shown in refs 31−33 that characteristics of auto-oscillation at the liquid/air interface are influenced by surfactant activity, solubility and bulk diffusion coefficients, liquid viscosity, density differences between the pure liquid and surfactant solution, and system dimensions (mainly by the cell radius and capillary immersion depth). The parameters responsible for the oscillations characteristics at the oil/water interface, in addition to those considered for the air/water interface, are (i) the surfactant partition coefficient between oil and water, (ii) the difference in densities between pure oil and oil surfactant solution (influencing the buoyancy in the oil phase), (iii) the viscosity and density of the oil phase, (iv) the surfactant diffusion coefficient in the oil phase, and (v) the height of the oil layer.

The numerical simulation shows that the surfactant partition coefficient has the strongest influence on the system evolution. The increase of the partition coefficient leads to an essential decrease of the oscillation amplitude. The oscillation period decreases as well, but its dependence on the partition coefficient is much less pronounced (see Figure 2 and Table 2). The oscillation amplitude becomes too small, and the oscillation

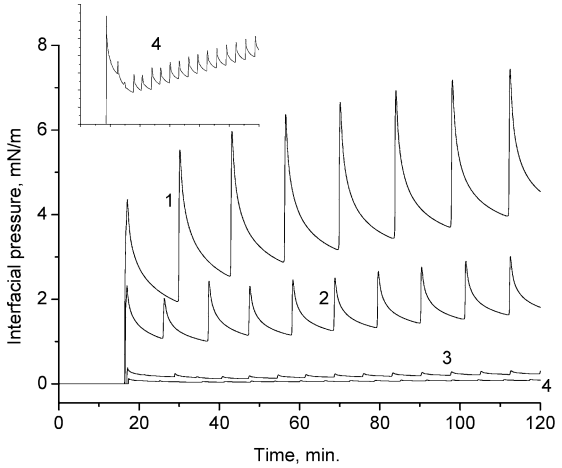

Figure 2. Dependence of the oscillation characteristics on the partition coefficient for the capillary immersion depth $h = 10$ mm (numerical results): $1 - k_p = 0$, $2 - k_p = 1$, $3 - k_p = 10$, and $4 - k_p = 30$.

TABLE 2: Dependence of the Auto-oscillations Characteristics on the Partition Coefficient

partition coefficient	induction period, min	oscillation period, min[a]	oscillation amplitude, mN/m[b]
0	16.4	14.2	4.4/3.5
1	16.5	10.8	2.3/1.3
10	17.0	7.0	0.38/0.067
30	17.3	6.1	0.13/0.021

[a] The mean value for the fifth−eighth oscillations. [b] Numerator, for the first oscillation; denominator, the mean value for the fifth−eighth oscillations.

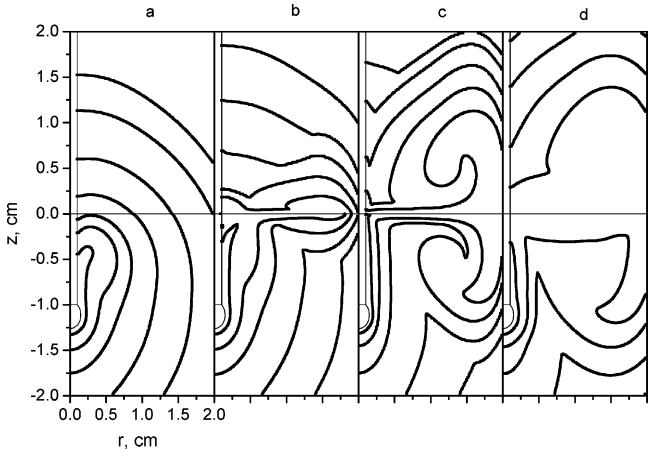

Figure 3. Dynamics of the concentration distribution in the bulk during the first oscillation for $k_p = 10$, $h = 10$ mm: $1 - t = 15$ min, $2 - t = 16$ min 59 s, $3 - t = 17$ min 9 s, and $4 - t = 20$ min (note, the concentration is constant along each curve but increases 10 times by crossing the interface, in accordance to the chosen value k_p).

should not become detectable in the experiment if the value of the partition coefficient is large enough.

Now, the hydrodynamic processes during the development of repeated oscillation of the interfacial tension at the liquid/liquid interface and the effect of the partition coefficient on these processes are considered in detail. At the beginning of the droplet dissolution, the interface is free of the surfactant and the interfacial pressure is equal to zero. The solute is transferred from the droplet to the interface by diffusion and buoyancy-driven convection. The solute distribution over the bulk is shown for this stage in Figure 3a. In the capillary region, there are deviations from the spherical distribution due to buoyancy-driven convection, whereas in more distant parts of the lower

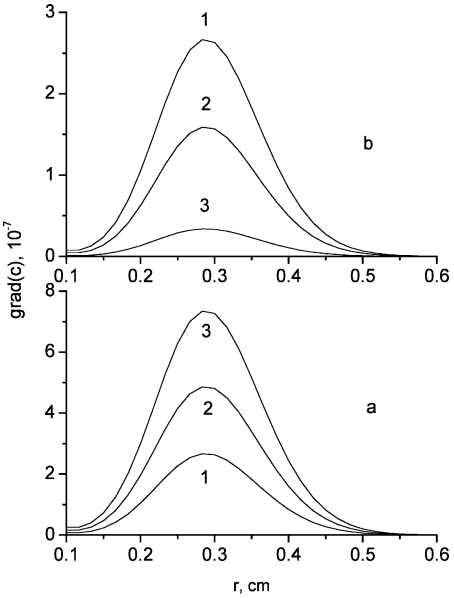

Figure 4. Dimensionless normal concentration gradients near the interface depending on the partition coefficients, (a) in the water phase, (b) the difference between the water and oil phases ($t = 15$ min): $1 - k_p = 0$, $2 - k_p = 1$, and $3 - k_p = 10$.

phase, as well as in the upper phase, the distribution is closer to spherical due to the predominance of diffusion mass transfer.

The surfactant concentration at the interface has a maximum in the capillary region and decreases very quickly in the direction to the wall, which means a surfactant concentration gradient arises at the interface and causes the development of convective motion due to the Marangoni effect (Figure 1). Initially, the Marangoni convection is very weak, and the mass transfer due to this convection is negligible in comparison to the mass transfer due to diffusion or buoyancy convection. At the same time, there is a feedback between the Marangoni convection and the concentration gradients in the system, which can result in the instability development.[30−32] It is obvious from the streamlines distribution, given in Figure 1, that the intensification of the Marangoni convection causes the reinforcement of the surfactant supply to the interface in the capillary region, the increase of the interfacial concentration gradient, and therefore, a further acceleration of the Marangoni convection.

The spontaneous acceleration of Marangoni convection, associated with the instability development, is only possible when the feedback becomes appreciable. This means that the contribution to the solute transfer due to Marangoni convection becomes comparable to that due to diffusion and buoyancy-driven convection. The source for a fast increase of the velocity of Marangoni-driven convection is the surfactant supply to the interface in the capillary region. Therefore, instability can develop in the system if the local maximum of the solute influx to the interface near the capillary exceeds a certain threshold value. This influx is the difference between the flux from the bulk water to the interface and that from the interface to the bulk oil (the last term in eq 5). So, it depends strongly on the partition coefficient. For a given time moment, the larger the partition coefficient, the larger the solute flux from the bulk water to the interface (Figure 4a). However, the larger the partition coefficient, the smaller the influx to the interface and the interfacial concentration Γ (Figure 4b). In Figure 4, the dimensionless values of the normal concentration gradients near the interface are presented. The diffusion fluxes are proportional to the concentration gradients because $D_1 = D_2$ in this study.

TABLE 3: Characteristics of the Instability Onset in the Systems with Different Partition Coefficients

partition coefficient, k_p	time of the instability onset	maximum grad(c) in water phase	maximum grad(c) in oil phase	difference of maximum grad(c) in water and oil phase
0	15 min 29 s	1.9×10^{-6}	0	1.9×10^{-6}
1	15 min 37 s	5.8×10^{-6}	3.9×10^{-6}	1.9×10^{-6}
10	16 min 4 s	42.9×10^{-6}	41.0×10^{-6}	1.9×10^{-6}
30	16 min 25 s	145.2×10^{-6}	143.1×10^{-6}	2.1×10^{-6}

The decrease of the influx to the interface with the increase of the partition coefficient causes a delay of the onset of instability. We estimated the time for the onset of instability for systems with different partition coefficients according to the minimum of the dependency $d \ln(c)/dt$ vs time[32] and compared the normal concentration gradients near the interface corresponding to these time moments. The results presented in Table 3 show clearly that the onset of instability corresponds to a certain value of the solute influx to the interface nearly independently of the partition coefficient. Obviously, the instability onset in the considered system can be related to the critical value of the local Marangoni number as it was made earlier for the air/water system.[32]

In the course of the instability development, the velocity as well as the solute transfer rate increases by some orders of magnitude. As shown in parts b and c of Figure 3, surfactant is spread over the interface and the interfacial pressure increases rapidly. The tangential concentration gradient increases, and the location of its maximum moves to the wall causing an increase of the surface velocity also in the wall region. At the same time, on the wall, the velocity is zero. Therefore, a large velocity gradient appears near the wall resulting in a contraction of the interface in this region. The surfactant concentration near the wall increases in comparison to the neighboring regions because the contraction is fast. Correspondingly, a reverse concentration gradient appears here. As a result, the surface velocity decreases and then, the liquid in the wall region begins to move in the direction from the wall to the capillary, forming the reverse convective roll, as shown in Figure 5a. Extending to the capillary region (parts b and c of Figure 5), the reverse roll breaks up the solute supply to the interface and the feedback supporting the Marangoni-driven convection disappears. The system returns to the slow stage of evolution, when the surfactant transfer occurs mainly by diffusion and buoyancy convection. In this stage, the surfactant gradually desorbs from the interface (Figure 3d) resulting in a decrease of the interfacial pressure. The return to the slow stage is the precondition for the following oscillation, which begins after the normal concentration gradient increases again, causing the development of the direct convective roll (with the interfacial velocity directed from the capillary to the wall) and suppression of the reverse roll (Figure 5d). The described mechanism of instability development is the same as in the air/water system described in detail elsewhere.[30]

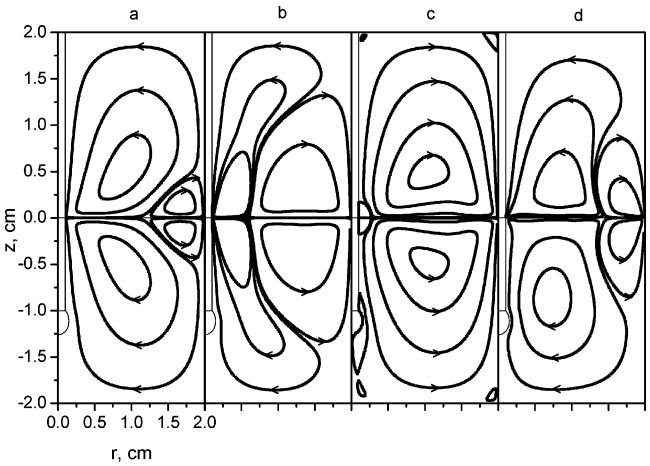

Figure 5. Dynamics of the streamlines distribution in the bulk during the first oscillation for $k_p = 10$, $h = 10$ mm: $1 - t = 17$ min 25 s, $2 - t = 17$ min 45 s, $3 - t = 18$ min, and $4 - t = 20$ min.

The oscillation amplitude is determined by the total amount of the surfactant supplied to the interface until the interfacial concentration begins to decrease. Figure 6 presents the time dependencies of the full solute fluxes over the interface, namely, the dimensionless quantities $F = 2\pi \int_0^1 \partial c/\partial z|_{z=0}\, r\, dr$ for each phase as well as their difference, for the systems with different partition coefficients. The beginning of the time intervals for each particular system is chosen in such a way that the abscissa $t = 5$ s corresponds to the moment when the maximum of the surface velocity in the middle of container is reached. To be precise, these maximums correspond to $t = 16$ min 30 s for $k_p = 0$, $t = 16$ min 38 s for $k_p = 1$, and $t = 17$ min 4 s for $k_p = 10$. Then, the beginning of time intervals in Figure 6 corresponds to the beginning of an appreciable increase of the surface pressure in each system, that is, to the beginning of the oscillation.

At the beginning of the oscillation, the difference in the solute supply from the lower phase to the interface for systems with different partition coefficients is comparatively small (Figure 6a). Then, the surfactant is spread very quickly over the interface, and the surface concentration increases in some orders of magnitude during a very short time (some seconds). The solute concentration in phase 2 still remains negligible at this time. Therefore, the larger the partition coefficient, the larger the mass flux from the interface to phase 2 (Figure 6b). At the time corresponding to the velocity maximum, $t = 5$ s, the full flux from the interface to the upper phase for $k_p = 10$ is 3.4 times larger than that for $k_p = 1$. As a result, the surfactant influx to the interface decreases as the partition coefficient increases. Moreover, in the system with a large partition coefficient, the surfactant removal from the interface to phase 2 exceeds quickly the supply of the surfactant from phase 1 to the interface and the interfacial concentration begins to decrease; whereas, in the system with a smaller partition coefficient, the surfactant influx to the interface still remains positive (Figure 6c). Thus, the sharp decrease of the oscillation amplitude with an increase of the partition coefficient is the result of the more intensive surfactant removal to the second phase during the fast stage and of the quicker decrease of the surfactant influx to the interface below zero. This results also in a faster return of the system to the slow stage of its evolution. The numerical simulation shows that the disappearance of the reverse roll occurs also quicker in systems with a large partition coefficient. Therefore, the oscillation period decreases as the partition coefficient increases (Table 2).

The intensification of the mass transfer in the upper phase due to an increase of the bulk diffusion coefficient is complementary to the effect of the partition coefficient (Table 4).

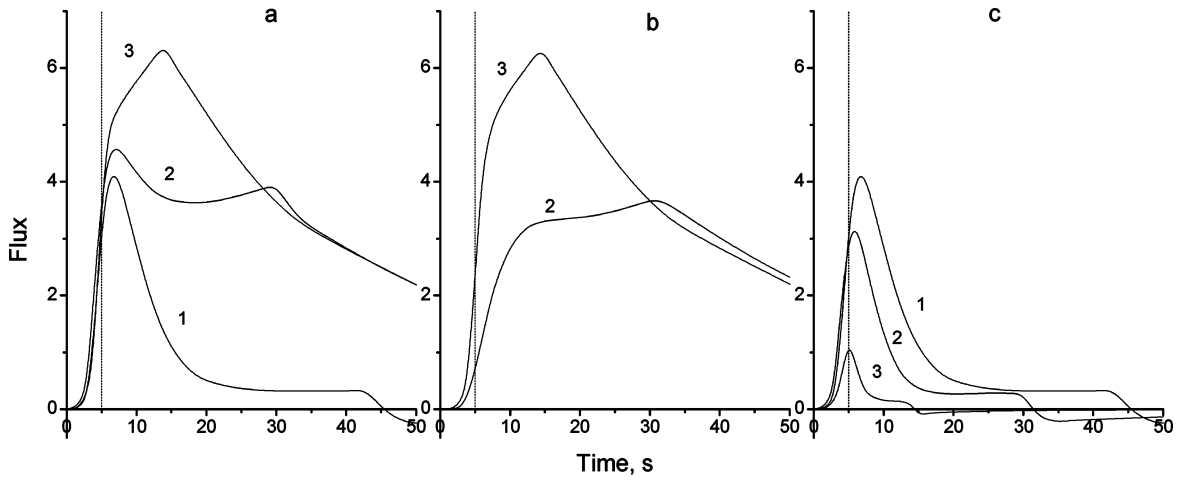

Figure 6. Dimensionless solute fluxes over the whole interface at the first oscillation: (a) flux from phase 1 to the interface, (b) flux from the interface to phase 2, and (c) flux difference a − b, $1 - k_p = 0$, $2 - k_p = 1$, and $3 - k_p = 10$.

TABLE 4: Dependence of the Oscillations Characteristics on the Solute Diffusion Coefficient in the Upper Phase ($k_p = 1$, $h = 10$ mm)

diffusion coefficient, cm^2/s	induction period, min	oscillation period, min[a]	oscillation amplitude, mN/m[b]
3.335×10^{-6}	16.5	12.2	2.9/2.1
6.67×10^{-6}	16.5	10.8	2.3/1.3
1.334×10^{-5}	16.6	9.4	1.7/0.7

[a] The mean value for the fifth−eighth oscillations. [b] Numerator, for the first oscillation; denominator, the mean value for the fifth−eighth oscillations.

TABLE 5: Dependence of the Oscillations Characteristics on the Upper Phase Viscosity and Density

upper phase kinematic viscosity, cm^2/s	upper phase density, g/cm^3	induction period, min	oscillation period, min[a]	oscillation amplitude, mN/m[b]
		$k_p = 0$, $h = 8$ mm		
0	1	12.7	13.16	3.9/3.5
0.01	1	13.3	13.23	4.1/3.5
0.1	1	14.4	13.26	4.6/3.5
0.1	0.1	13.3	13.21	4.1/3.5
		$k_p = 10$, $h = 10$ mm		
0.001	1	16.3	6.4	0.33/0.060
0.01	0.1	16.3	6.9	0.36/0.064
0.01	1	17.0	7.0	0.38/0.067

[a] The mean value for the fifth−eighth oscillations. [b] Numerator, for the first oscillation; denominator, the mean value for the fifth−eighth oscillations.

To study the effect of the viscosity of the upper phase on the oscillation characteristics, we have varied the kinematic viscosity of the oil phase in the range of 0−0.1 cm^2/s and its density in the range of 0.1−1 g/cm^3 (Table 5). The increase of the dynamic viscosity, $\mu_2 = \rho_{02}\nu_2$, results in an increase of the induction period, since the larger the dynamic viscosity of the upper phase, the larger the influx of the solute to the interface should be reached for the onset of instability. A similar increase of the induction period is caused also by an increase of the lower phase viscosity.[32] Period and amplitude of the oscillations are nearly independent of the upper phase viscosity for the partition coefficient $k_p = 0$. The dependence becomes more significant as the partition coefficient increases. The increase of the dynamic viscosity leads to the increase of the period and amplitude of the oscillation, which means its effect opposes the effect of the partition coefficient. It should be stressed that an increase of only kinematic viscosity by keeping dynamic viscosity constant also results in an increase of the oscillation period and amplitude, but the effect is weaker.

TABLE 6: Dependence of the Oscillations Characteristics on the Density Difference between the Pure Liquid and Saturated Surfactant Solution in the Upper Phase ($k_p = 10$)

density difference, g/cm^3	induction period, min	oscillation period, min[a]	oscillation amplitude, mN/m[b]
0	17.0	7.0	0.38/0.067
−0.001	17.0	6.8	0.38/0.067
−0.01	17.0	6.5	0.38/0.069
0.01	17.0	8.0	0.38/0.066

[a] The mean value for the fifth−eighth oscillations. [b] Numerator, for the first oscillation; denominator, the mean value for the fifth−eighth oscillations.

It was shown in ref 33 that the buoyancy force due to the dependency of the solution density on its concentration influences strongly the oscillation characteristics at the air/water interface. According to the results of numerical simulations, already the density difference of 1×10^{-6} g/cm^3 between water and saturated surfactant solution results in a noticeable decrease of the oscillation period in comparison to systems where the buoyancy is absent. The influence of the density difference in the upper liquid phase is not so strong, since during the process the concentration difference in the upper phase remains much smaller than that in the lower phase near the droplet. The effect can be neglected for density differences less than 10^{-3} g/cm^3 (Table 6). A density difference large enough causes a decrease of the oscillation period when the surfactant solution is heavier than the pure liquid 2 and an increase of the oscillation period in the opposite case. The dependence of the oscillation amplitude on this parameter is rather weak. The induction period is independent of the density difference as, at this stage, the surfactant concentration in the second phase is negligible.

The characteristics of auto-oscillations at the air/water interface depend on the system geometry (capillary immersion depth, radius and depth of the cell, and droplet radius).[21,31,33] In the case of the oil/water system, there is an additional geometrical parameter, namely, the depth of the upper liquid layer which influences the mass transfer processes in the upper phase and, thus, can change the oscillation characteristics. The results, presented in Table 7, show that the decrease of the upper layer depth results in the increase of period and amplitude of the oscillation. However, the effect is rather weak for the values of $H_2 \geq 5$ mm. The induction period and the amplitude of the

TABLE 7: Dependence of the Oscillation Characteristics on the Height of the Upper Liquid Layer

partition coefficient	layer height, mm	induction period, min	oscillation period, min[a]	oscillation amplitude, mN/m[b]
1	20	16.5	10.8	2.3/1.3
1	10	16.5	11.2	2.3/1.4
1	5	16.6	11.7	2.35/1.5
30	20	17.3	6.1	0.13/0.021
30	10	17.3	6.5	0.13/0.027

[a] The mean value for the fifth−eighth oscillations. [b] Numerator, for the first oscillation; denominator, the mean value for the fifth−eighth oscillations.

first oscillation are practically independent of this parameter due to the negligible amount of surfactant in the upper phase during the induction period.

It is worth to note that the effect of the boundary condition for the vortex at the upper boundary of the oil phase is negligible in the considered range of the upper layer depths. The simulations performed display that, even for $H_2 = 5$ mm, the difference in the results obtained with no-slip and free boundary conditions is less than 2%.

Comparison with Experiment. The performed experiments show that the dissolution of an alcohol droplet under the heptane/water interface results in oscillations of the interfacial tension very similar to those observed at the air/water interface. In the following, for these two systems, the expected differences in the oscillations characteristics are discussed on the basis of the theoretical analysis presented above.

First of all, the surfactant activity at the oil/water interface differs from that at the air/water interface. Interfacial properties of aliphatic alcohols at the heptane/water interface were studied in ref 37 to estimate the free energy of adsorption. Unfortunately, the data immediately concerning the surfactant properties are not presented, but the activity values, defined as

$$\alpha = \lim_{c \to 0} \frac{1}{RT}\left(\frac{\pi}{c}\right) \tag{9}$$

can be recalculated from the given values of adsorption energy (here π is the interfacial pressure). The results of the recalculations are listed in Table 8 together with the data for alcohol activities at the air/water interface taken from ref 19.

It is seen that the activity of alcohols at the heptane/water interface is higher than that at the air/water interface. The activity increase should lead to a comparably moderate increase of the oscillation period and amplitude, as shown experimentally[19] and theoretically.[32]

The partition coefficient is another parameter with a strong effect on the oscillation characteristics. The data of partition coefficients between water and *n*-alkanes C_8H_{18}, $C_{12}H_{26}$, and $C_{16}H_{34}$ for alcohols from C_4H_9OH to $C_7H_{15}OH$ are given in ref 36. We extrapolated the results of ref 36 to heptane used in our experiments. The value of the partition coefficient for octanol is obtained by subsequent extrapolation of the results for alcohols from butanol to heptanol and should be considered only as an estimation. The corresponding values of the partition coefficients are presented in Table 8.

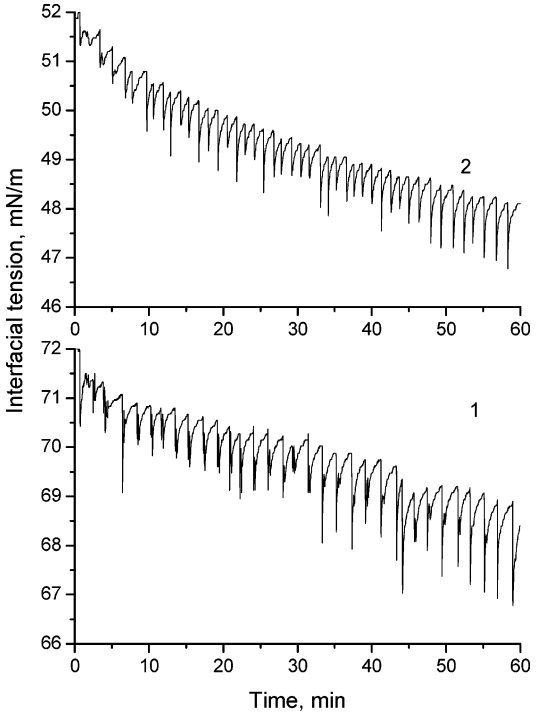

Figure 7. Auto-oscillations of the surface tension produced by a hexanol droplet, $h = 12$ mm: (1) air/water interface, (2) heptane/water interface.

The partition coefficient for hexanol is in the order of unity; therefore, the oscillations produced by the hexanol droplet at the air/water and oil/water interfaces should not considerably differ, especially taking into account the increase of the hexanol activity by replacing air by oil. At the same time, the oscillations, produced by the octanol droplet, should have a much smaller amplitude and, possibly, a little smaller period at the heptane/water interface in comparison to the air/water interface, according to the large partition coefficient of octanol at the heptane/water interface. In this case, the increase of activity and the presence of the second viscous phase have, obviously, a much smaller effect on the amplitude than the increase of the partition coefficient. There is also some difference in the bulk diffusion coefficients of alcohols in heptane and the density difference between heptane and saturated alcohol solution, which reinforces the effect of the partition coefficient for long-chain alcohols. It should be stressed that the effect of the large diffusion coefficient in the air in comparison to that in heptane can be neglected because of the large difference in the partition coefficients, as proved by the numerical simulations.

The experimental results, presented in Figures 7 and 8, confirm these conclusions. The values of oscillation period differ only slightly at the oil/water and air/water interfaces for both alcohols, whereas the difference in oscillation amplitude depends strongly on the alcohol used. The oscillation amplitudes for hexanol are rather close in both systems considered, whereas

TABLE 8: Physicochemical Properties of Aliphatic Alcohols

alcohol	activity at heptane/water interface, cm	activity at air/water interface, cm	partition coefficient between heptane and water	diffusion coefficient in heptane,[a] 10^{-5} cm^2/s	density difference between heptane and saturated alcohol solution,[b] 10^{-3} g/cm^3
hexanol	2.26×10^{-4}	1.43×10^{-4}	2.1	2.6	−2.0
octanol	5.36×10^{-3}	2.13×10^{-3}	40	2.2	−3.1

[a] The values are calculated employing the Wilke−Cang correlation.[38] [b] The values are calculated for ideal solutions.

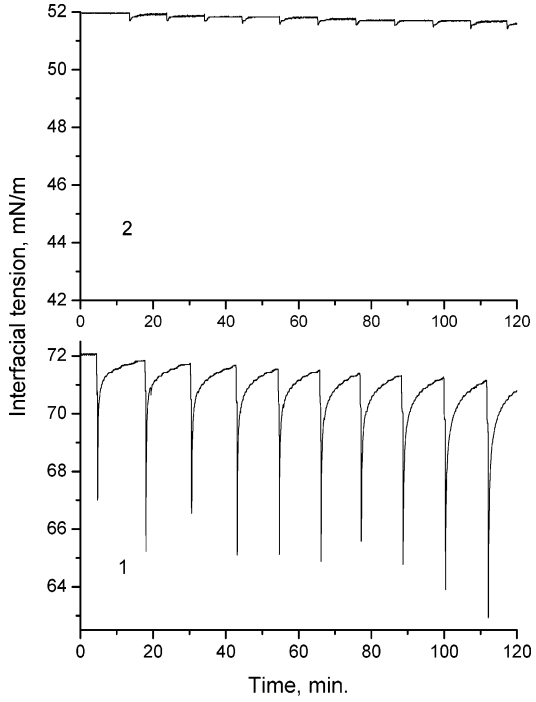

Figure 8. Auto-oscillations of the surface tension produced by an octanol droplet, $h = 8$ mm: (1) air/water interface, (2) heptane/water interface.

for octanol, the amplitude at heptane/water interface is already 20−30 times smaller than that at the air/water interface. Summarizing, these experimental results are in good qualitative agreement with the theory.

Conclusions

Dissolution of a surfactant droplet under the oil/water interface results in auto-oscillations of the interfacial tension, which are very similar to the auto-oscillations observed at the air/water interface. The results of numerical simulations show that auto-oscillations at both types of interfaces are governed by nearly the same mechanism, considered in detail in the preceding papers;[30−33] namely, they are the result of the Marangoni instability, periodically arising and fading in the system.

The surfactant partition coefficient affects very strongly the characteristics of surface tension auto-oscillations at the liquid/liquid interface. An increase of the partition coefficient leads to a decrease of the oscillation period and, especially, the amplitude. The other physicochemical and geometrical properties of the second liquid phase, such as, the difference in densities between pure oil and surfactant solution in oil, viscosity and density of the oil phase, surfactant diffusion coefficient in the oil phase, and the height of the oil layer have a minor effect on the characteristics of the oscillations.

The theoretically predicted strong dependence of the oscillation characteristics on the partition coefficient is in a good qualitative agreement with the experiments.

Acknowledgment. N.M.K. thanks the MPI of Colloids and Interfaces for financial support. Financial assistance from the National Ukrainian Academy of Sciences is gratefully acknowledged.

References and Notes

(1) Nakache, E.; Dupeyrat, M. In *Convective transport and instability phenomena*; Zieper, J., Oertel, H., Eds.; Braun: Karlsruhe, Germany, 1982; p 319.
(2) Kai, S.; Mori, T.; Miki. M. In *Pattern formation in complex dissipative Systems;* Kai, S., Ed.; World Scientific: River Edge, NJ, 1992; p 144.
(3) Arai, K.; Kusu, F. In *Liquid interfaces in chemical, biological and pharmaceutical applications (Surf. Sci. Series/95)*; Volkov, A. G., Ed.; Marcel Dekker Inc: New York, 2001; p 699.
(4) Srivastava, R. C.; Rastogi, R. P. Transport mediated by electrified interfaces. Studies in the linear, nonlinear and far from equilibrium regimes. In *Studies in Interface Science*; Möbius, D., Miller, R., Eds.; Elsevier: Amsterdam, The Netherlands, 2003; Vol. 18.
(5) Kovalchuk, N. M.; Vollhardt, D. *Prog. Colloid Polym. Sci.* **2004**, *128*, 36.
(6) Dupeyrat, M.; Nakache, E. *Bioelectrochem. Bioenerg.* **1978**, *5*, 134.
(7) Nakache, E.; Dupeyrat, M.; Vignes-Adler, M. *J. Colloid Interface Sci.* **1983**, *94*, 187.
(8) Nakache, E.; Dupeyrat, M.; Vignes-Adler, M. *Faraday Discuss. Chem. Soc.* **1984**, *77*, 189.
(9) Magome, N.; Yoshikawa, K. *J. Phys. Chem.* **1996**, *100*, 19102.
(10) Shioi, A.; Sugiura, Y.; Nagaoka, R. *Langmuir* **2000**, *16*, 8383.
(11) Shioi, A.; Kumagai, H.; Sugiura, Y.; Kitayama, Y. *Langmuir* **2002**, *18*, 5516.
(12) Shioi, A.; Katano, K.; Onodera, Y. *J. Colloid Interface Sci.* **2003**, *266*, 415.
(13) Yoshikawa, K.; Matsubara, Y. *J. Am. Chem. Soc.* **1984**, *106*, 4423.
(14) Arai, K.; Fukuyama, S.; Kusu, F.; Takamura, K. *Electrochim. Acta* **1995**, *40* (18), 2913.
(15) Pimienta, V.; Lavabre, D.; Buhse, T.; Micheau, J. C. *J. Phys. Chem. B* **2004**, *108*, 7331.
(16) Yoshihisa, H.; Sutou, S.; Miyamura, K.; Gohshi, Y. *Anal. Sci.* **1998**, *14*, 133.
(17) Srividhya, J.; Gopinathan, M. S. *J. Phys. Chem. B* **2003**, *107*, 1438.
(18) Kovalchuk, V. I.; Kamusewitz, H.; Vollhardt, D.; Kovalchuk, N. M. *Phys. Rev. E* **1999**, *60*, 2029.
(19) Kovalchuk, N. M.; Vollhardt, D. *J. Phys. Chem. B* **2000**, *104*, 7987.
(20) Kovalchuk, N. M.; Vollhardt, D. *Mater. Sci. Eng. C* **2002**, *22*, 147.
(21) Grigorieva, O. V.; Kovalchuk, N. M.; Grigoriev, D. O.; Vollhatdt, D. *J. Colloid Interface Sci.* **2003**, *261*, 490.
(22) Takahashi, T.; Yui, H.; Sawada, T. *J. Phys. Chem. B* **2002**, *106*, 2314.
(23) Yui, H.; Ikezoe, Y.; Takahashi, T.; Sawada, T. *J. Phys. Chem. B* **2003**, *107*, 8433.
(24) Ikezoe, Y.; Ishizaki, S.; Yui, H.; Fujinami, M.; Sawada, T. *Anal. Sci.* **2004**, *20*, 435.
(25) Ikezoe, Y.; Ishizaki, S.; Takahashi, T.; Yui, H.; Fujinami, M.; Sawada, T. *J. Colloid Interface Sci.* **2004**, *275*, 298.
(26) Sternling, C. V.; Scriven, L. E. *AIChE J.* **1959**, *5*, 514.
(27) Sørensen, T. S.; Hennenberg, M.; Sanfeld, A. *J. Colloid Interface Sci.* **1977**, *61*, 62.
(28) Reichenbach, J.; Linde, H. *J. Colloid Interface Sci.* **1981**, *84*, 433.
(29) Chu, X.-L.; Velarde, M. G. *J. Colloid Interface Sci.* **1989**, *131*, 471.
(30) Kovalchuk, N. M.; Vollhardt, D. *Phys. Rev. E* **2002**, *66*, 026302.
(31) Kovalchuk, N. M.; Vollhardt, D. *J. Phys. Chem. B* **2003**, *107*, 8439.
(32) Kovalchuk, N. M.; Vollhardt, D. *Phys. Rev. E* **2004**, *69*, 016307.
(33) Kovalchuk, N. M.; Vollhardt, D. *J. Phys. Chem B* **2005**, *109*, 15037.
(34) Roache, P. J. *Computational Fluid Dynamics*; Hermosa: Albuquerque, NM, 1976.
(35) Azouni, M. A.; Normand, C.; Petre, G. *J. Colloid Interface Sci.* **2001**, *239*, 509.
(36) Aveyard, R.; Mitchell, R. W. *Trans. Faraday Soc.* **1969**, *65*, 2645.
(37) Vilallonga, F. A.; Koftan, R. J.; O'Connel, J. P. *J. Colloid Interface Sci.* **1982**, *90*, 539.
(38) Reid, R. C.; Prausnitz, J. M.; Sherwood. T. K. *The Properties of Gases and Liquids*; McGraw-Hill: New York, 1977.